Accepted Manuscript
Version of Record at: https://doi.org/10.1021/acs.jpcc.4c03849

Photoexcited Energy Relaxation in Porphyrin Nanorings

Kennet J. Rueda Espinosa and Alexei A. Kananenka*

Department of Physics and Astronomy, University of Delaware, Newark, Delaware 19716, United States

E-mail: akanane@udel.edu

Accepted Manuscript
Version of Record at: https://doi.org/10.1021/acs.jpcc.4c03849

Abstract

Natural photosynthetic systems convert solar energy to chemical energy with extremely high efficiency. Synthetic chromophore arrays are promising models for understanding and mimicking energy migration in natural light-harvesting systems. To duplicate the structure and function of natural systems, a multitude of cyclic porphyrin arrays have been synthesized over the past decades. In a recent breakthrough [*Nat. Chem.* **2022**, *14*, 1436–1442], synthetic butadiyne-linked porphyrin nanorings have been shown to exhibit excitation energy transfer on the same timescale and length scale as the natural light-harvesting complex LH2 and with comparable efficiency. In the pursuit of understanding the fundamental underpinnings of the exciton dynamics in such systems we combined time-dependent density functional theory with the hierarchical equation of motion approach and performed a systematic study of population dynamics, coherence length, and the energy transfer in linear and cyclic multiporphyrin nanostructures with and without the butadiyne moiety. In a very good agreement with experiments, we showed that the ultrafast delocalization process of the exciton in symmetric structures occurs during the first 300 fs after the excitation. Migration and localization of the excitation in segments with π-conjugation links happens on a timescale of tens of picoseconds. We also found that coherence length dynamics in multiporphyrin systems is very robust to the environmental effects. Another notable feature of butadiyne-linked porphyrin nanorings is that the energy transfer efficiency can exceed 80%.

I Introduction

Throughout the history of mankind nature has been providing continuous inspiration to humans for developing new technologies. One notable example which has always been elusive is photosynthesis in plants and bacteria with its remarkable, exceeding 95%, efficiency in channeling the excitation energy from multiple chromophores to a single collector in the reaction center of a photosynthetic complex. The natural light-harvesting complex LH2 is the primary antenna complex of the chromatophore of purple photosynthetic bacteria *Rhodobacter sphaeroides*. After the initial absorption of light by the pigments of LH2 complex, the excitation energy is passed

between LH2, LH1 (light harvesting complex I), and the reaction center (RC). At the RC, the energy is used for charge separation, thus forming an electrical gradient across the membrane and initiating the next step in photosynthetic energy trapping.[1] LH2 is formed by a ring of nine copies of a $\alpha\beta$-heterodimer. Bound to each $\alpha\beta$-heterodimer are 3 bacteriochlorophyll (BChla) and 1 carotenoid molecules for a total of 36 pigments in LH2.[2] The near-IR absorption spectrum of LH2 shows two distinct peaks, due to the BChla in the complex, at 800 and 850 nm.[2] The 800 and 850 nm peaks are due to the Q_Y excited states of BChla located in the B800 and B850 rings of LH2. The BChls in the B800 band are sufficiently far apart so that they interact only weakly with each other, thus each absorbs individually.[3] The BChls of the B850 ring are tightly packed, with center-to-center distances of less than 1 nm, and thus interact strongly with each other to form delocalized exciton states, shifting the absorption peak of the ring to 850 nm.[2] Energy that is absorbed by the B800 BChls or carotenoid is quickly transferred to the B850 exciton states which then transfer it to exciton states of nearby LH2 and LH1 complexes.[4] The intraring exciton energy transfer (EET) occurs faster than 200 fs. This system has inspired a vast number of efforts to synthesize cyclic artificial molecular systems with enhanced light-harvesting properties based on multiporphyrin arrays.[5–10] However, despite decades of work aiming to achieve EET efficiencies in artificial systems comparable to their natural counterparts, EET in these systems is still generally slower than in the LH2 complex.

Multiporphyrin systems are amenable to customization by changing their shapes, geometries, sizes, and by incorporating other functional molecular units into the porphyrin framework. This creates an immense range of porphyrin nanostructures that can be tested as candidates for mimicking natural photosynthetic systems. In a recent breakthrough, nanorings composed of closely spaced exciton-coupled porphyrin units were synthesized and the excitation dynamics in these systems was studied.[11] It was demonstrated experimentally that *ca.* 30% of the EET in these systems occurs within 350 fs and the final transfer efficiency was estimated to exceed 93%. The key insight was to incorporate the butadiyne moiety into the porphyrin ring to control the energy flow. This exciting advancement represents a significant leap towards creating artificial systems

Accepted Manuscript
Version of Record at: https://doi.org/10.1021/acs.jpcc.4c03849

mimicking the natural LH2 complex.

Simulations, including electronic-structure calculations and quantum dynamics approaches are indispensable in the molecular design of artificial light-harvesting systems. Even though multiple theoretical models have been proposed to explain the optical properties of multiporphyrin systems, there is currently lack of understanding of the excitation energy dynamics and relaxation in these structures.[12–15] This is in stark contrast to natural photosynthetic systems such as LH2 and Fenna–Matthews–Olson complex, that have been extensively studied using the large variety of quantum, classical, semiclassical, and mixed quantum-classical methods.[16–25]

Here, we study the excitation and energy relaxation in the porphyrin nanorings of various sizes with and without the butadiyne linker. A series of model Hamiltonians were parametrized using time-dependent density functional theory. Numerically exact hierarchy of equations of motion (HEOM)[26,27] method was used calculate quantum dynamics in these systems. We compare the population dynamics and exciton localization in such systems to linear multiporphyrin chains. We found that the ultrafast excition delocalization occurs on the timescale of few hundreds of femtoseconds, in agreement with experiments.[11,28] For the porphyrin nanoring system with the butadiyne linker, the initial delocalization is followed by an incoherent energy transfer to the lowest energy porphyrin sites connected to the linker. This process occurs on the timescale of tens of picoseconds. Additionally, we investigate how the size of the system, temperature, and system-environment coupling affect the excition dynamics and delocalization in such systems.

II Methods

We studied the excitation dynamics in porphyrin nanorings with and without the butadiyne linker and in linear porphyrin chains. Each system studied was denoted using the following notation: *a*-P*N*(*b*), where *a* denotes either cyclic '*c*' or linear '*l*' porphyrin ('P') system of *N* porphyrin units and '*b*' indicates whether a (single) butadiyne linker is present. Even though the main focus of this Article is the excitation dynamics in butadiyne-linked cyclic multiporphyrin structures, it is worth

Accepted Manuscript
Version of Record at: https://doi.org/10.1021/acs.jpcc.4c03849

comparing it to the dynamics of linear and cyclic porphyrin nanorings. The following systems were studied: cyclic porphyrin nanorings *c*-P*N* with N = 9, 12, 24, and 36 units; cyclic porphyrin systems with the butadiyne linker *c*-P*N*b with N =12 and 24; linear porphyrin chains *l*-P*N* with N=9, 12, 18, and 24 units.

A multiporphyrin system comprised of N porphyrin units (molecules) joined together is described by the following excitonic Hamiltonian

$$\hat{H}_S = \sum_{n=1}^{N} E_n |n\rangle\langle n| + \sum_{n=1}^{N}\sum_{m=1}^{N} V_{nm} |n\rangle\langle m|, \tag{1}$$

where $|n\rangle$ represents the excitation localized on nth porphyrin unit, with E_n being the corresponding excitation energy, and V_{nm} is the coupling between the nth and mth units. The absorption spectrum of porphyrin is characterized by two representative high- and low-energy peaks, referred to as the B (Soret) and Q bands, respectively. Here we focus on the Q transition, therefore E_n is the corresponding excitation energy of this band. The Q transition is directed through the axis that connects each porphyrin unit with its neighbor and, in cyclic porphyrin arrays, the direction of the transition dipole moments is parallel or "head to tail",[29] as illustrated in Figure 1 for the *c*-P24*b* system.

Geometries of all the circular and linear multiporphyrin systems were taken from ref 11. Monomers and *l*-P2b dimers, including 3,5-bis(octyloxy)phenyl solubilizing groups (Figure S1) were obtained from the multiporphyrin structures by carving out one or two units, respectively, and capping broken bonds with hydrogen atoms.

In multiporphyrin systems and, in the absence of static disorder, the excitation energy of all sites is taken to be the same $E_n \equiv E_Q$, where E_Q is the Q excitation energy of the porphyrin molecule in a given solvent. E_Q transition energies were calculated using time-dependent density functional theory (TDDFT) within the Tamm–Dancoff approximation.[30] Toluene was chosen as a solvent and was modeled using the polarizable continuum model (PCM).[31] Previous studies of the photophysical properties of porphyrin monomers showed that B3LYP functional[32,33] reproduces the experimental energies of the Q transition. However, studies on chlorophyll

Accepted Manuscript
Version of Record at: https://doi.org/10.1021/acs.jpcc.4c03849

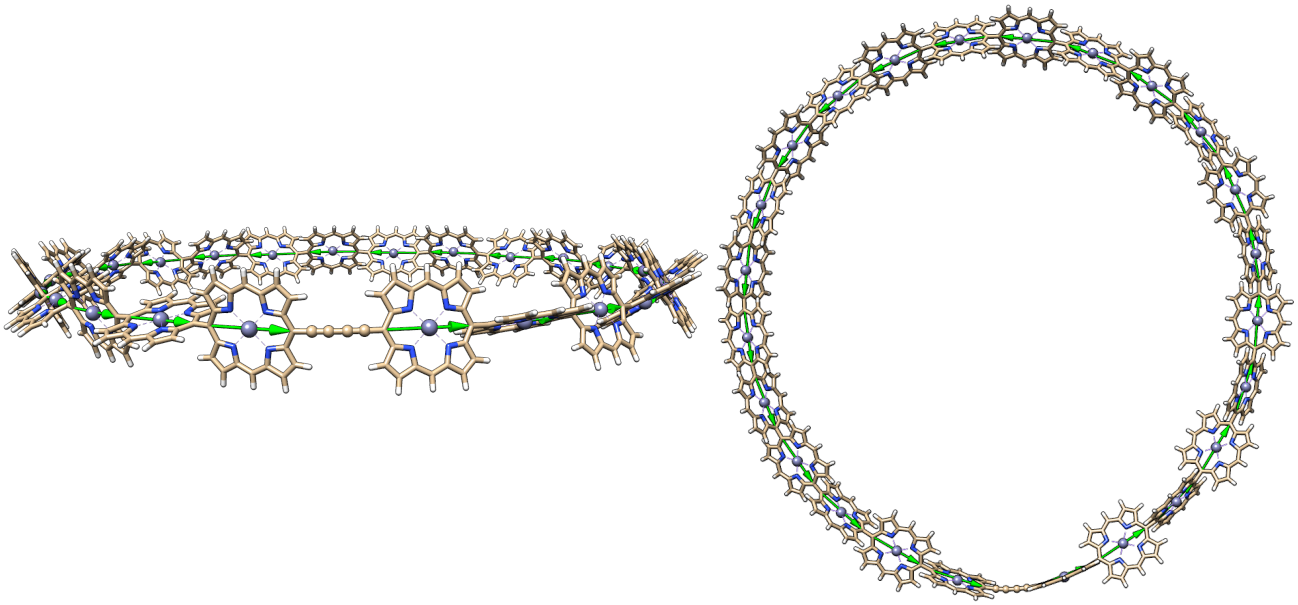

Figure 1. *c*-P24b porphyrin nanoring comprising 24 porphyrin units and a butadiyne linker. The arrows show the Q transition dipole moments.

(Chla) molecules have shown that TDDFT generally overestimates the excitation energies and B3LYP functional generates spurious transitions. CAM-B3LYP[34] and ωB97X-D3[35] produce excitation energies in better agreement with experiment, although they still suffer from the fiction-excitation-level problems.[36,37] Other studies benchmarking density functional approximations on biochromophores have shown that the PBE0[38] functional and other recently developed hybrid functionals with a larger Hartree–Fock exchange contribution correctly reproduce the vertical excitation energies.[39] Here we tested three functionals B3LYP, CAM-B3LYP, ωB97X-D3, and PBE0 functionals with def2-TZVP[40] basis set were used by calculating E_Q transition energies. Best performing functional was used parametrization of the Hamiltonian, eq 1. All TDDFT calculations were performed using Q-CHEM package.[41]

In the presence of the butadiyne linker, the excitation energy of the two porphyrin units immediately connected to the linker, which we denote as E_b, cannot be the same as E_Q of a single porphyrin molecule. To determine E_b, TDDFT calculations for the butadiyne linked porphyrin dimer, *l*-P2*b*, were performed with various functionals and the value closest to the experimental was taken. The excitation energies of all porphyrin fragments that are two or more units away

Accepted Manuscript
Version of Record at: https://doi.org/10.1021/acs.jpcc.4c03849

from the butadiyne moiety are assumed to be the identical and equal to E_Q determined as described above.

The coupling between the porphyrin monomers is described by the dipole-dipole interaction

$$V_{nm} = g\frac{\mu_\varepsilon^2}{R_{nm}^3}\left[\vec{e}_n \cdot \vec{e}_m - 3\left(\vec{e}_n \cdot \vec{e}_{nm}\right)\left(\vec{e}_m \cdot \vec{e}_{nm}\right)\right], \tag{2}$$

where $\vec{e}_n$ is a unit vector along the transition dipole moment of the nth porphyrin molecule, the unit vector $\vec{e}_{nm}$ is oriented along the line connecting the centers of the nth and mth porphyrin units, R_{nm} is the corresponding distance, and μ_ε^2 is the dipole strength of the Q transition of the porphyrin in the medium with dielectric constant ε, g is the screening factor, which is taken to be $1/\varepsilon$, with $\varepsilon = 2.38$ for toluene.[42]

Dipole-dipole coupling is a reasonable approximation for the non-nearest monomers given that the distance between the porphyrin molecules in the array is larger than the extent of their ground and excited state wave functions.[43] For the nearest neighbors, previous experimental works on meso-meso linked porphyrins have shown that the dipole approximation is still valid although it can underestimate the coupling value.[44] Another issue is that TDDFT predicts the oscillator strengths and transition dipole moments for the Q band in monomers that are too low less than $1D$ for all density functionals tested here (see Figure S2). To model the transition dipole moment of the porphyrin unit more accurately, we used the experimental value of the coupling between meso-meso porphyrins V_{ij} =570 cm^{-1} derived from the Q-band[44] and inverted eq 2 to find μ_ε. The direction of the transition dipole moment was taken from TDDFT calculations. We found it to be essentially parallel to the axis that connects the monomers. The final derived value $\mu_\varepsilon = 8.9$ D (in toluene). Experimental values for transition dipole moments in zinc porphyrins are around 7.5 D[45]so we find our derived value reasonable.

The total Hamiltonian of the system and the bath is given by

$$\hat{H} = \hat{H}_s + \hat{H}_b + \hat{H}_{sb}, \tag{3}$$

Accepted Manuscript
Version of Record at: https://doi.org/10.1021/acs.jpcc.4c03849

where the second and third terms describe the bath (thermal reservoir) and system-bath coupling, respectively. We model the bath as a collection of N_b quantum harmonic oscillators

$$\hat{H}_b = \sum_{j=1}^{N_b} \left(\frac{\hat{p}_j^2}{2m_j} + \frac{1}{2} m_j \omega_j^2 \hat{x}_j^2 \right), \tag{4}$$

which are independently coupled to the Q excited state of each porphyrin unit. In eq 4 $\hat{p}_j, \hat{x}_j, m_j$, and ω_j are the momentum, position, mass, and frequency of the jth harmonic oscillator, respectively. The system is assumed to be linearly coupled to the bath

$$\hat{H}_{sb} = \sum_{n=1}^{N} \sum_{j=1}^{N_b} c_j \hat{x}_j \hat{R}_n, \tag{5}$$

where $\hat{R}_n = |n\rangle\langle n|$ and the coupling constants c_j are characterized by the bath spectral density which is assumed to be identical for all porphyrin units

$$J(\omega) = \frac{\pi}{2} \sum_{j=1}^{N_b} \frac{c_j^2}{m_j \omega_j} \delta\left(\omega - \omega_j\right). \tag{6}$$

The reduced density matrix of the multiporphyrin system $\hat{\rho}_s(t)$ is obtained by tracing out the bath degrees of freedom

$$\hat{\rho}_s(t) = \mathrm{Tr}_b[\hat{\rho}(t)], \tag{7}$$

where $\hat{\rho}$ is the density operator of the total system.

The dynamics of the reduced density matrix of the porphyrin system can be given in the form of the formally exact time-ordered influence functional, as follows in 8 when the bath follows Gaussian statistics

$$\hat{\rho}_s(t) = \mathscr{T}_{\leftarrow} \exp\left\{ -\frac{1}{\hbar^2} \int_0^t dt_2 \int_0^{t_2} dt_1 \left\langle \mathscr{L}_{sb}(t_1)\, \mathscr{L}_{sb}(t_2) \right\rangle_B \right\} \hat{\rho}_s(0), \tag{8}$$

where $\mathscr{L}_{sb\cdot} = \left[\hat{H}_{sb}, \cdot\right]$ is the system's Liouvillian superoperator, $\langle\cdot\rangle_B = \mathrm{Tr}_b\left[\cdot e^{-\beta \hat{H}_b}\right]/Z$ is a thermal quantum-mechanical average over bath modes, $\beta = (k_B T)^{-1}$ is the inverse temperature, (k_B is

Accepted Manuscript
Version of Record at: https://doi.org/10.1021/acs.jpcc.4c03849

the Boltzmann constant), $Z \equiv \mathrm{Tr}_b\left[e^{-\beta \hat{H}_b}\right]$ is the partition function, and $\mathscr{T}_{\leftarrow}$ orders $\mathscr{L}_{sb}(t)$'s in increasing time from right to left.

In this work the spectral density for the bath local to every porphyrin site is chosen to be an overdamped Drude-Lorentz spectral density[46]

$$J(\omega) = 2\lambda \frac{\gamma\omega}{\gamma^2 + \omega^2}, \tag{9}$$

where λ is the reorganization energy and γ is the cut-off frequency of the bath.

The initial state of the total system in dynamics simulations corresponds to the factorized state $\hat{\rho}(0) = \hat{\rho}_s(0) \otimes \hat{\rho}_b^{eq}$, where the porphyrin system's initial density operator is given by $\hat{\rho}_s(0) = |i\rangle\langle i|$ which corresponds to a single, ith, porphyrin site being initially excited. The site i that is excited depends on the type of system and will be specified in Sec. III. The bath is assumed to be in its thermal equilibrium $\hat{\rho}_b^{eq} = e^{-\beta \hat{H}_b}/\mathrm{Tr}\left[e^{-\beta \hat{H}_b}\right]$. This factorized state is valid since it arises from photon-induced ground-to-excited state transition according to Frank–Condon principle.[17,47] For linear porphyrin chains, two initial states of the porphyrin subsystem system were considered: the one in which the terminal porphyrin unit is excited and the one with the central porphyrin unit is initially excited.

The population and coherence dynamics following the initial excitation were studied over 2 ps. The coherence length as a measure of the excition localization was calculated as the inverse participation ratio[48]

$$L_\rho = \frac{1}{N} \frac{\left(\sum_{nm} |\rho_{nm}|\right)^2}{\sum_{nm} |\rho_{nm}|^2}, \tag{10}$$

where ρ_{nm} denotes the elements of the system's reduced density matrix.

The bath parameters were chosen as follows. In ref 49, the reorganization energy for the zinc-porphyrin dimers in toluene was previously measured to be in the range of 100-200 cm^{-1}, where 70-90 cm^{-1} is due to the solvent. Therefore, we set to $\lambda = 100\ \mathrm{cm}^{-1}$ and $\gamma = 60\ \mathrm{ps}^{-1}$. In addition, to explore the effect of the environment on the population dynamics and exciton delocalization, we also used the reorganization energy previously reported for the LH2 complex $\lambda = 200\ \mathrm{cm}^{-1}$, and

Accepted Manuscript
Version of Record at: https://doi.org/10.1021/acs.jpcc.4c03849

a larger value of $\lambda = 400$ cm^{-1}.[17] We note that these parameters are site-independent because of the assumption mentioned earlier that each porphyrin unit is subjected to the identical bath. Given the high symmetry of most of the systems under study this is a reasonable assumption.

An accurate description of the excitation dynamics in multiporphyrin systems requires non-perturbative quantum dynamics approaches because the intersite porphyrin-porphyrin couplings are similar to the system-bath couplings. In this work, the dynamics of the system was propagated using numerically exact Hierarchy of equations of motion (HEOM) method[26,27] as implemented in the PHI package.[50] The hierarchy truncation level L and the number of Matsubara terms M were set to 4 and 3, respectively. The integration time step was set to 0.5 fs. We verified that the population dynamics was converged with respect to L by setting L=3, 4 and 5 in a *c*-P9 system with M=3. Similarly, the convergence with respect to M was verified by using M=1, 2, and 3, with H=4. As shown in Figure S3, the population dynamics is identical in all cases.

III Results and discussion

A Hamiltonian parameters

E_Q was determined by calculating the excitation energy of a porphyrin monomer and butadiyne-linked dimer *l*-P2*b* using TDDFT with B3LYP, CAM-B3LYP, ωB97X-D3, and PBE0 functionals and def2-TZVP basis set. Results are summarized in Table 1.

Table 1: Q excitation energies (in eV) E_Q of the isolated porphyrin molecule (monomer) and the butadiyne-linked porphyrin dimer. $\Delta E = E_{\mathbf{monomer}} - E_{l-\mathbf{P2}b}$.

Functional	Excitation energy		ΔE
	monomer	*l*-P2*b*	
B3LYP	2.358	1.895	0.462
CAM-B3LYP	2.396	2.096	0.299
PBE0	2.396	1.956	0.441
ωB97x-D3	2.363	2.122	0.241

The calculated absorption spectrum for the monomer is presented in Figure S4. A well-defined

Accepted Manuscript
Version of Record at: https://doi.org/10.1021/acs.jpcc.4c03849

low-energy excited state corresponding to the Q band is observed for all the functionals tested. As shown in Table 1 all functionals used here predict nearly the same value of the Q excitation energy for the monomer. We note that the discrepancy in the excitation energies of higher excited states is clearly significant among the tested functionals, but they are not relevant for the following discussion. The two major Q and Soret bands are better described by ωB97x-D3 and CAM-B3LYP functionals.

Absorption spectra of the *l*-P2b dimer calculated using the same functionals are shown in Figure S4. The lower energy state is attributed to the presence of the butatyne linker and the corresponding excitation energy, E_b, which is used in our model Hamiltonian as the excitation energy for the *l*-P2b dimer fragment of the *c*-PNb rings. The presence of this peak is consistent with the photophysical description of the dimer.[11,51] There is a considerable scatter in the E_b excitation energies for the *l*-P2b dimer predicted by the functionals used here, as shown in Table 1. Experimental estimate for the difference between the Q transition energy of a *l*-P24 and the lower peak of the *c*-P24b spectrum is *ca.* $\Delta E = 0.25$ eV.[11] ΔE calculated using ωB97x-D3 functional agrees very well with the experiment. Because ωB97x-D3 functional is also accurate for the E_Q energies we choose to parametrize the Hamiltonian based on ωB97x-D3 calculations. Therefore, we set $E_Q = 2.363$ eV and $E_b = 2.122$ eV.

B Ultrafast excitation dynamics and coherence length

We begin by discussing the population dynamics in the linear *l*-P*N* structures. To study the effect of the chain length, two systems were studied with $N = 24$ and $N = 9$ porphyrin units. The results are shown in Figure 2. Figures 2 (a) and (b) show the population dynamics after one terminal porphyrin unit was initially excited (site 1). The excitation rapidly delocalizes and an extended wave packet travels through the chain which is evident by growing populations of intermediate sites seen in Figures 2 (a) and (b), until it reaches another end of the chain, site N.

The timescale of this process is size-dependent, as expected. In the $N = 9$ case the terminal unit's population spikes at 50 fs while it takes 120 fs for the excitation to reach the other end of the

Accepted Manuscript
Version of Record at: https://doi.org/10.1021/acs.jpcc.4c03849

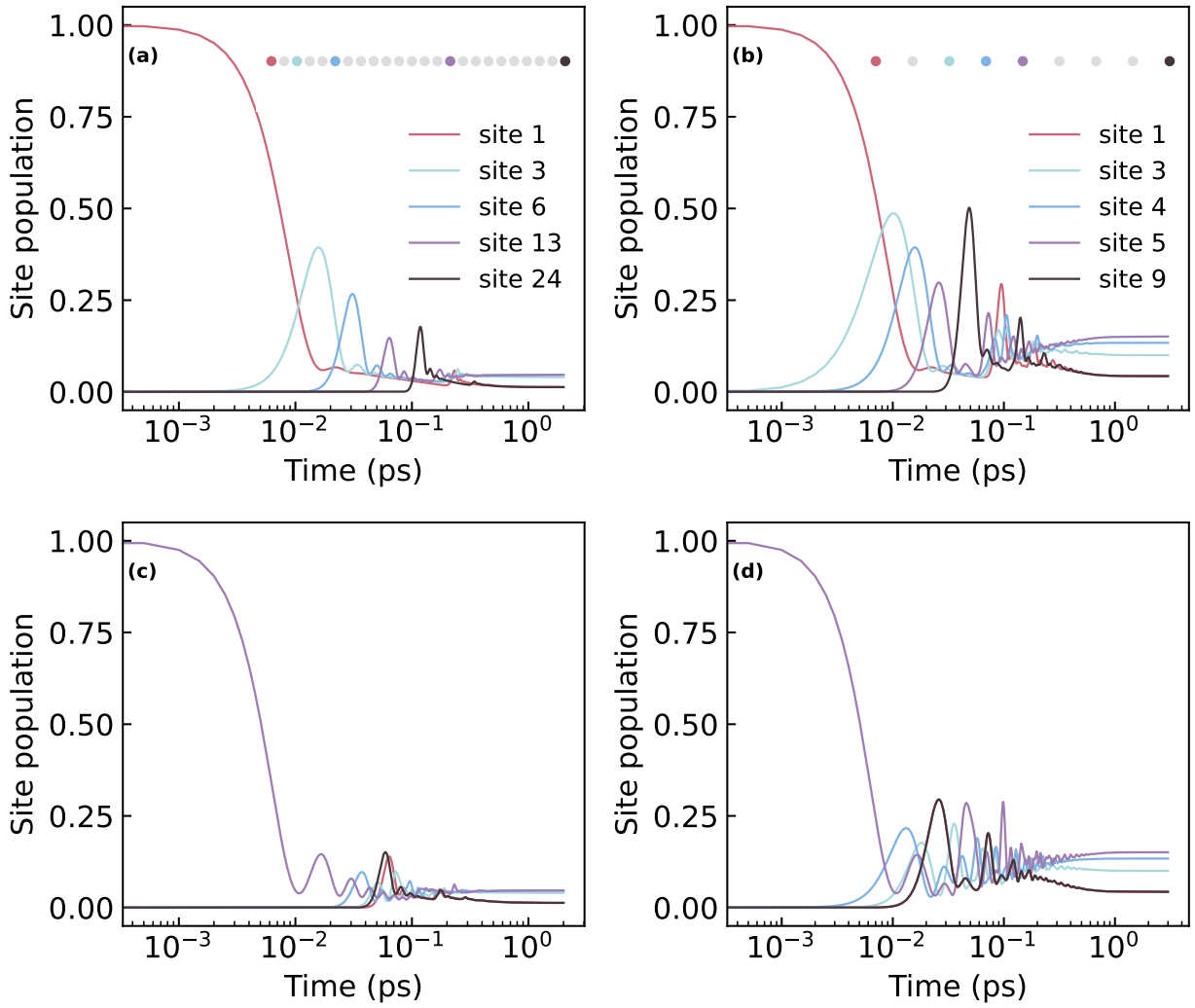

Figure 2. Site populations for the linear porphyrin chains of the two sizes *l*-P24 (left) and *l*-P9 (right) and two initial states: (a), (b) with the site at the end of the chain being initially excited and (c), (d) with the central porphyrin unit being initially excited. The insets show the locations of the sites whose population dynamics is reported (colored circles). Temperature is 300 K.

Accepted Manuscript
Version of Record at: https://doi.org/10.1021/acs.jpcc.4c03849

l-P24 system. After reaching the end, the excitation is reflected and travels back to the originally excited porphyrin unit reaching it at around 140 fs and 320 fs for $N = 9$ and $N = 24$ systems, respectively as evidenced by small fading revivals in the population of site 1. Small spikes in the population of the terminal porphyrin unit occurring even before the reflected excitation reaches the initially excited site again, is likely due to the interaction between reflected and the residual tail of the incoming wave packets. After the initial delocalization the dynamics becomes complex with multiple interferences between the wave packets indicated by the rapid spikes in the populations. Interaction with the environment dampens the oscillations until the population reaches a stationary value. This behavior has been found and discussed as a signal of coherent transport by others in similar systems.[52]

Figures 2 (c) and (d) present the population dynamics after the central porphyrin unit is initially excited. For the *l*-P24 system the 13th porphyrin unit was initially excited. In this case, the excitation spreads over symmetrically towards both ends of the porphyrin chain reaching terminal units faster compared to the previously discussed case where a terminal unit was initially excited. For *l*-P9 and *l*-P24 systems the timescale for reaching the end of the system are 25 and 60 fs, respectively. Because now the excitation spreads evenly to both ends of the molecule the population of a single terminal unit is less as seen in Figures 2(c), (d). After reflection at the end of the chain the excitation reaches the central porphyrin unit again which, for the *l*-P24 occurs in 110 fs. In *l*-P9 system this dynamical process clearly repeats at least twice with the end of the chain gaining a considerable population at 25 fs which is then transferred to the central unit by 50 fs. Then, again, in another cycle, the excitation comes back to the central unit at 100 fs. This process continues until the populations reach their stationary values.

The population dynamics of the *l*-P24 system is somewhat less rich. In the absence of the dissipative environment *l*-P24 system will of course show the same wave packet dynamics but on a longer timescale. Because of the environment, however, the populations in the *l*-P24 system coherently oscillate only until *ca.* 300 fs. During this time the excitation travels to the end of the chain and, essentially, never comes back as there is no cosiderable population spike in the central

Accepted Manuscript
Version of Record at: https://doi.org/10.1021/acs.jpcc.4c03849

unit occuring before the populations reach their stationary values.

The equilibrium populations expectedly do not depend on where the initial excitation is localized. This final populations follow the symmetry of the system with the central porphyrin unit carrying most of the population while the terminal units are the least populated. The time to reach the steady populations is shorter for larger rings. This is because, in shorter porphyrin chains, the wave packet interferences are more likely to occur and lead to spikes in the populations. Dissipative environment affect the dynamics by localizing the wave packet which is more efficient in the larger porphyrin chains.

The population dynamics in cyclic multiporphyrin systems without the butadiyne linker (*c*-P*N*) is illustrated in Figure 3 for $N = 9$, 12, 24, and 32. Initially the excitation was localized at a single porphyrin unit. Figure 3a reports the population dynamics of the initially excited site. The population dynamics of the site that is diametrically opposite to it is illustrated in Figure 3b.

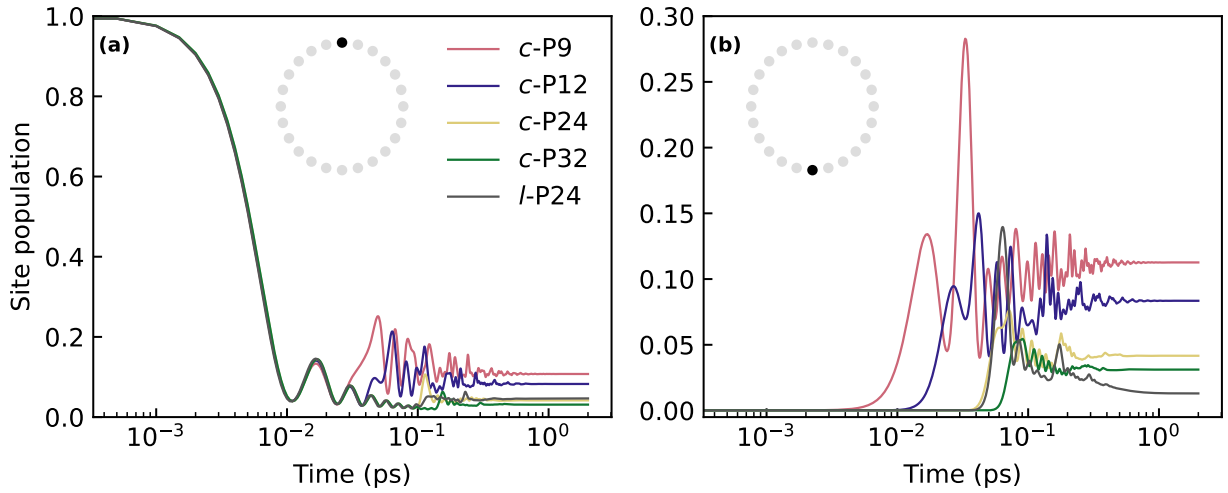

Figure 3. Population dynamics in cyclic multiporphyrin systems *c*-P*N* with $N = 9$, 12, 24, and 32 and a linear system *l*-P24. Shown are the populations of the initially excited site (a) and its antipodal (diametrically opposite) site (b). The insets show the two relevant sites for the *c*-P24 system. For the linear multiporphyrin system panel (b) reports the population of the terminal unit on the other end of the chain with respect to the initially excited site.

As seen in Figure 3 the excitation rapidly delocalizes in both directions from the initially excited porphyrin site. This is clearly seen as the initial population dynamics, $t < 30$ fs, is system-independent. The two branches of the wave packet spreading in the opposite directions interfere at

Accepted Manuscript
Version of Record at: https://doi.org/10.1021/acs.jpcc.4c03849

the porphyrin site diametrically opposite (antipodal) the site of the initial excitation. This process depends on the size of the ring occurring earlier in the smaller rings, as expected. For example, the first spike in the population of the antipodal site occurs as early as 16 fs in the smallest ring studied with $N = 9$ units. It is in the $N = 9$ system that the population of this site is largest. This is because the excitation delocalizes over fewer sites in the smaller system with each site gaining more population. The next significant event occurs when the wave packet completes its first lap which occurs at 30 fs for $N = 9$ system and is evidenced by the spike in the population of the site of the initial excitation. The same dynamics is observed for *c*-P12 system except it is delayed due to the bigger size. The antipodal site is reached at 25 fs and it takes 46 fs to complete the first revolution. The population dynamics in bigger systems follows the same trend. The population dynamics of linear and cyclic systems with the same number of porphyrin units, e.g., *l*-P24 and *c*-P24 systems, can be compared by analyzing Figure 3. In the first 100 fs the dynamics of the two systems is identical and corresponds to the excitation delocalization. According to Figure 3 the time to reach the diametrically opposite site in the *c*-P24 system is the same as the time to reach the terminal unit in the linear *l*-P24 system. The topology: circular vs linear has no effect on the early ultrafast dynamics in multiporphyrin systems (the initial state will, of course, have). At *ca.* 100 fs the population of the initially excited site increases only slightly for the linear chain but it is much more significant in the case of a cyclic *c*-P24 system. This is because in the cyclic system two wave packets travelling in the opposite directions interfere again at the initially excited site.

The equilibrium populations in *c*-P*N* systems are larger for the smaller systems as expected. The equilibrium population of the initially excited in the *c*-P24 system is close that of *l*-P24 system, while the population of the antipodal and terminal sites in the respective systems are clearly different. The population of the terminal units in the linear porphyrin chain is small due to the topology effect.

Experiments have shown that in π-conjugated macrocycle nanorings with up to 24 porphyrin units, the delocalization occurs in the first 200 fs after absorption.[28] The same process studied in meso-meso-linked porphyrin systems has been reported to occur faster than 350 fs.[11] If we define

Accepted Manuscript
Version of Record at: https://doi.org/10.1021/acs.jpcc.4c03849

the delocalization time as the time required to reach the steady-state population then for the *c*-P24 system, we found that the delocalization process takes *ca.* 400 fs. Therefore, our simulations are in a reasonable agreement with the experimental results.

Coherence length is a measure of the exciton delocalization. In Figure 4(a) the coherence length, calculated using eq 10, for *l*-P24, *c*-P24 and *c*-P24b systems are compared. The coherence length dynamics for all systems is similar in the first 800 fs and it goes through a series of sharp spikes. Similarly to the population dynamics discussed above, this increase in the coherence length is due to wave packet spreading and interference. After each drop the coherence length never rises up to the value before the drop due to dissipation exerted by the environment. Therefore, the largest coherence length of 17 units is achieved only after the initial excitation. This value also agrees with the our previous observation that the earlier ultrafast dynamics in multiporphyrin systems does not depend on the system's topology. However, as we discuss below it depends on the initial state of the system. After a series of ultrafast spikes the coherenence length dynamics in the cyclic and linear systems slowly rises up to its equilibrium value on the timescale of 1 ps. During this time the environmental-assisted merge of the two wave packets occurs. In case of cyclic structures the two wavepackets are moving clockwise and counter clockwise, while for linear structures it is the two wave packets that move to the either end that merge.

The equilibrium coherence length for the *c*-P24 system is 13 porphyrin units. This value can be compared to other cyclic structures such as LH2 for which coherence length is 11 [17] and thiophene-based macrocycles for which it is 18.[53] The equilibrium coherence length for the linear structure *l*-P24 is 10.5 which is smaller compared to the cyclic system comprised of the same number of porphyrin units (*c*-P24). This, again, can be explained by the consequence of the topology causing vanishingly small population of the terminal units for linear porphyrin chains.

Coherence length dynamics in the linear structure depends on the initial state of the system, as shown in Figure 4. When one terminal porphyrin unit of the linear chain is initially excited the wave packet can only spread in one direction and, thus, the coherence length cannot get larger compared to when the central porphyrin unit is excited. The equilibrium coherence length is,

Accepted Manuscript
Version of Record at: https://doi.org/10.1021/acs.jpcc.4c03849

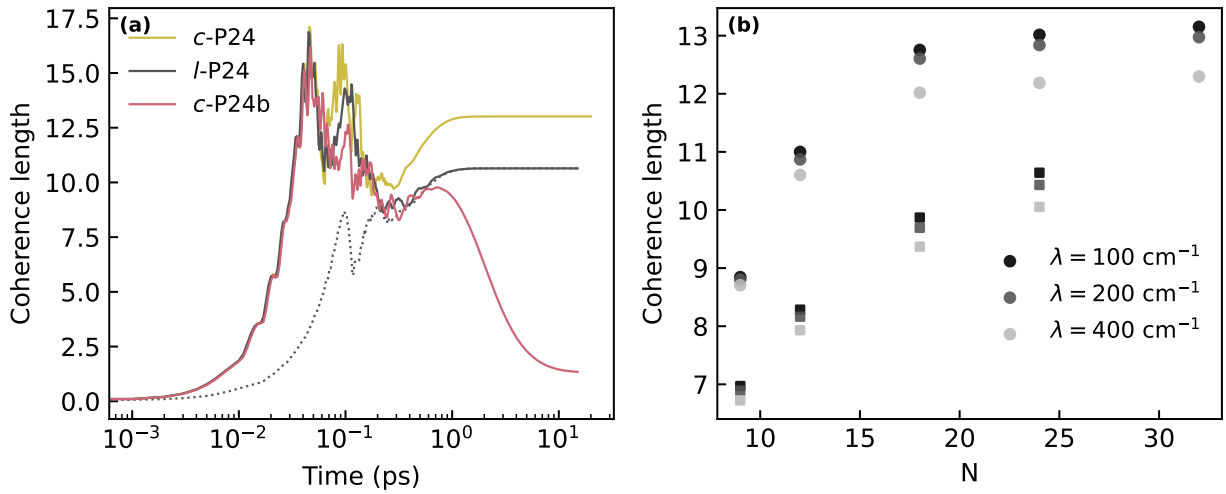

Figure 4. (a) Coherence length as a function of time for the *c*-P24, *c*-P24b, and *l*-P24 systems. Two initial conditions were considered for the linear *l*-P24 system: the central porphyrin unit is excited (solid black line) and one of the terminal porphyrin units is excited (dotted black line). (b) Equilibrium values of the coherence length for the *c*-PN systems with N = 9, 12, 18, 24, and 32 structures (circles) and the *l*-PN systems with N = 9, 12, 18, and 24 linear chain (squares) calculated for different reorganization energies of the environment. The temperature was set to 300 K in all calculations.

however, independent of the initial excitation, as expected.

Figure 4(b) reports the equilibrium coherence length for the rings (circles) and linear chains (squares) of different sizes. The equilibrium coherence length was calculated at 4.0 ps when the system has reached the stationary state. For the rings with $N < 12$ units, the coherence length is approximately the same size as the ring size $L_\rho \approx N$ meaning that the system is highly coherent. When the number of porphyrin units increases, the coherence length eventually saturates at 13 units. The saturation of the coherence length with respect to the size of the system has been experimentally observed before in linear porphyrin chains.[54] The reported experimental value is between 4 and 5 units which is notably smaller than the value obtained here. Interestingly, nearly identical discrepancy between experimental and HEOM predictions has been observed before for the LH2 system with the experimental coherence length of 4.1[44] being lower than the theoretical value of 11.[17] We believe that this discrepancy is due to the absence of the disorder, vibronic coupling, and more realistic spectral densities in our model.[55,56] Other measurements of

Accepted Manuscript
Version of Record at: https://doi.org/10.1021/acs.jpcc.4c03849

the coherence length can be used (e.g., refs 55,56), which could yield lower estimates for most of the parameters. They, however, depend on the temperature and, crucially, the inhomogeneous disorder, which is often ignored in the simulations but may be important. Addressing this issue would require methods beyond the scope of this Article and will be published elsewhere.

In addition, the effect of the coupling to the environment on the coherence length was explored by changing the bath reorganization energy λ. The results are shown in Figure 4(b). Increase in the system-bath coupling (larger bath reorganization energy) leads to the larger degree of exciton localization and, therefore, the coherence length decreases. Overall, the coherence length is, however, very robust to the changes in the system-bath coupling. For example, for the *c*-P24 ring the fourfold increase in the reorganization energy leads to the reduction of the coherence length by only one unit. On a related note, experiments on *c*-P*N* nanorings similarly reported that the excitation dynamics in these systems is remarkably robust against disorder-induced weakening of the electronic coupling between porphyrin units.[28]

C Donor-acceptor dynamics in butadiyne-linked porphyrin nanorings

Finally, we focus on the excitation dynamics in porphyrin nanoring systems with the butadiyne linker, *c*-PNb. In these systems, the excitation energy of the two porphyrin units directly connected to the butadiyne linker is lower compared to the rest of the porphyrin sites. This leads to the directional energy transfer and localization of the excitation in this porphyrin butadiyne-linked porphyrin "dimer" denoted as *l*-P2*b*. Figure 5(a) shows the population dynamics of the several selected sites of the *c*-P24b system, including the *l*-P2*b* dimer. Two initial states were considered: the initial excitation is localized on the diametrically opposite site to the butadiyne linker (solid lines, figure 5a,b) and the initial excitation is fully delocalized with equal amplitude on all porphyrin units except the two that are directly connected to the butadiyne linker (dashed lines). The latter initial condition approximately simulates a broadband excitation of the dense manifold of excited states separated from the two lowest excited states that correspond to the excitation localized at the two porphyrin sites connected to the butadiyne linker. In case where the

Accepted Manuscript
Version of Record at: https://doi.org/10.1021/acs.jpcc.4c03849

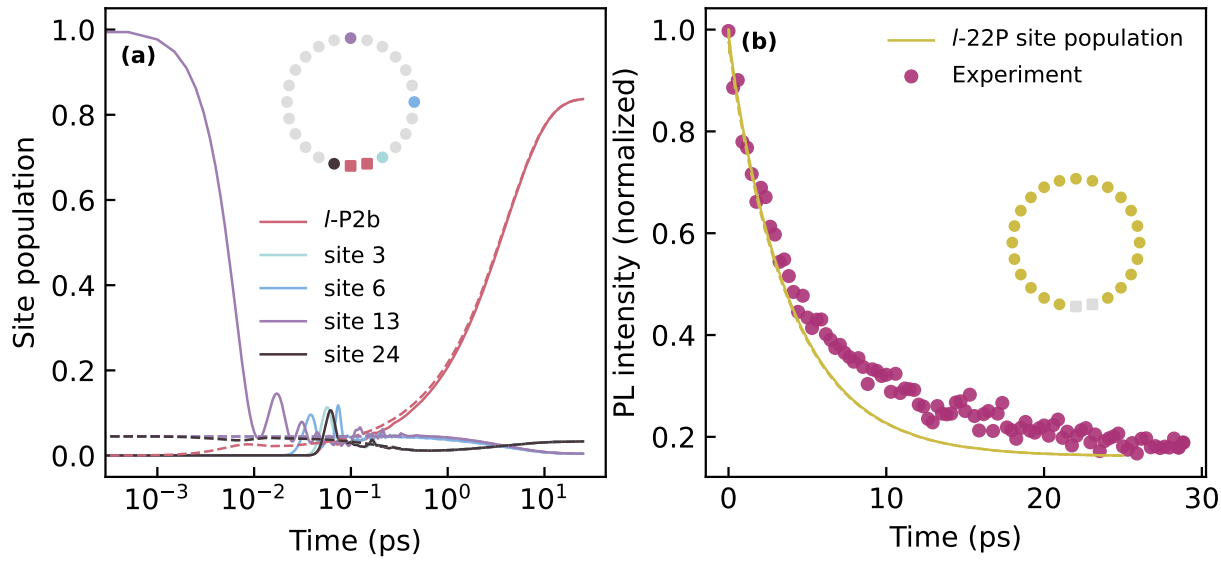

Figure 5. (a) Population dynamics for the *c*-P24b system. (b) Transient photoluminescence (PL) intensity at $\lambda = 720$ nm taken from ref 11 (purple circles) compared to the calculated population of the meso-meso-linked porphyrins. Solid lines correspond to the initial state where the diametrically opposite site (purple, see inset) is excited; dashed lines correspond to the initial state where all porphyrin units, except for the two connected to the butadiyne linker, are coherently excited.

diametrically opposite site to the linker is excited, the ultrafast excition delocalization occurred in the first 400 fs, similar to the cyclic symmetric porphyrin *c*-P24 system. The difference is that in the butadiyne-linked system the population is then incoherently transferred to the porphyrin dimer near the linker on a much slower timescale of tens of picoseconds (*ca.* 30 ps). At 25 ps, 84% of the population was transferred to the butadiyne-linked porphyrin dimer, and the rest of the excitation was distributed between the remaining porphyrin units in the ring. When the initial excitation is delocalized over all porphyrin units but the two connected to the linker, the signatures of the ultrafast initial delocalization are no longer present as expected. The population transfer to the porphyrin dimer is essentially identical to that of the case where only one porphyrin unit is initially excited as shown in Figure 5.

At this point it is worth discussing the connection between *c*-P24b and LH2 systems. The delocalization of the excitation across porphyrin units in the *c*-P24*b* system is similar to the *intraring* exciton delocalization in the B850 ring of the LH2 system and occurs on the same timescales. The longer-time transfer from porphyrins of the ring to the butadiyne-linked porphyrin

Accepted Manuscript
Version of Record at: https://doi.org/10.1021/acs.jpcc.4c03849

dimer can be considered similar to the *interring* excitation transfer between the B850 rings.[17]

Coherence length dynamics in a cyclic porphyrin system with the butadiyne linker is similar to the dynamics in other systems up to 1 ps as shown in Figure 4. The excitation is then localized in the *l*-P2b fragment of the chain as a result of its lower energy. The corresponding final coherence length is 1.3 units. Similar dynamics is observed for the *c*-P12b system as illustrated in Figure S5. The same ultrafast delocalization and energy transfer process occurs in the same timescales. Interestingly, unlike in the bigger *c*-P24b system, the transference process for the smaller system starts even before the population reaches its stationary value.

Gotfredsen *et al.*[11] used ultrafast time-resolved photoluminescence (PL) spectroscopy to study the intramolecular energy transfer in the *c*-P24*b* system. They observed a time-dependent shift of the emission from 690 to 730 nm in the first 500 ps after excitation of *c*-P24*b*. In agreement with our simulations they interpreted the early-time PL spectra as originating from the individual meso-meso linked porphyrin units, and the time-dependent shift as representative of the energy transfer dynamics to the butadiyne-linked porphyrin unit. They also found that the coupled dynamics in *c*-P24*b* emission detected at 650 and 720 nm can be used to describe the population dynamics of the donor and acceptor, respectively.[11] In Figure 5(b) we compare the calculated total population in the *c*-P24*b* ring less the population of the sites of the butadiyne-linked dimer to the experimentally measured PL spectrum at 720 nm. Agreement with the experiment is excellent which indicates that our approach correctly simulates the dynamics and excitation energy transfer in butadiyne-linked porphyrin nanorings.

The energy transfer efficiency reported by Gotfredsen *et al.*[11] is 93%. There is more than one definition of the efficiency. If we define the efficiency as the population transferred from the sites which are not part of the *l*-P2b dimer to the dimer, then our estimate of the efficiency would be 84%. This is in a good agreement with experiment, although one has to be mindful that different definitions of the efficiency are likely to give different estimates.

Accepted Manuscript
Version of Record at: https://doi.org/10.1021/acs.jpcc.4c03849

IV Conclusions

The excitation dynamics of chains and rings of closely spaced porphyrin molecules were investigated using time-dependent density functional theory and hierarchy of equations of motion approaches. We parametrized model Hamiltonians describing the interacting multiporphyrin systems coupled to the dissipative environment. We also studied recently synthesized cyclic multiporphyrin systems containing a single butadiyne linker introduced to direct the energy flow.[11] Such system is a very promising synthetic counterpart of the natural light-harvesting complex LH2. We studied the population dynamics and exciton delocalization followed the initial excitation. We found that the exciton delocalization occurs in all the systems faster than 300 fs. For the porphyrin nanorings, larger rings reach a thermal state faster than the smaller ones because coherent oscillations due to population interference are less present and the effect of the bath is more pronounced. The extent of exciton delocalization, measured by the coherence length L_ρ reached a maximum equilibrium value of 13 units, independent of the size of the system, but is found to be sensitive to how the initially excited Frank–Condon state was prepared. For the cyclic system of porphyrin units with a butadiyne unit, the linker acts as an acceptor site. An incoherent energy transfer to this butadiyne-linked porphyrin dimer acceptor unit occurs in the order of tens of picoseconds. The simulated timescales agree well with experimental results. This work establishes a computationally inexpensive yet accurate framework for studying the excitation energy transfer in conjugated systems with different topologies. Multiporphyrin systems such as *c*-P24*b* studied here are promising frameworks for artificial light-harvesting. Robust and accurate simulation methods might be the key for future rapid technological advances. In future publications we will extend our approach to larger systems which are rapidly gaining attention.[57]

Acknowledgement

This work is supported by the U.S. Department of Energy, Office of Science, Office of Basic Energy Sciences, under Award Number DE-SC0024511. A.A.K. also acknowledges the start-up funds provided by the College of Arts and Sciences and the Department of Physics and Astronomy of the University of Delaware. Calculations were performed with high-performance computing resources provided by the University of Delaware.

Supporting Information Available

Parametrized system Hamiltonians, structures of the porphyrin monomer unit and the *l*-P2b dimer, TDDFT absorption spectra of the porphyrin monomer and the *l*-P2b dimer, convergence of the population dynamics for *c*-P9, population dynamics and coherence length as a function of time for the *c*-P12b system.

References

(1) Hunter, C.; Daldal, F.; Thurnauer, M.; Beatty, J. *The Purple Phototrophic Bacteria*; Advances in Photosynthesis and Respiration; Springer Netherlands, 2008.

(2) Koepke, J.; Hu, X.; Muenke, C.; Schulten, K.; Michel, H. The crystal structure of the light-harvesting complex II (B800–850) from Rhodospirillum molischianum. *Structure* **1996**, *4*, 581–597.

(3) Hu, X.; Ritz, T.; Damjanović, A.; Schulten, K. Pigment Organization and Transfer of Electronic Excitation in the Photosynthetic Unit of Purple Bacteria. *The Journal of Physical Chemistry B* **1997**, *101*, 3854–3871.

(4) Hu, X.; Ritz, T.; Damjanović, A.; Autenrieth, F.; Schulten, K. Photosynthetic apparatus of purple bacteria. *Quarterly Reviews of Biophysics* **2002**, *35*, 1–62.

(5) Aratani, N.; Kim, D.; Osuka, A. Discrete Cyclic Porphyrin Arrays as Artificial Light-Harvesting Antenna. *Accounts of Chemical Research* **2009**, *42*, 1922–1934.

(6) Cho, H. S.; Rhee, H.; Song, J. K.; Min, C.-K.; Takase, M.; Aratani, N.; Cho, S.; Osuka, A.; Joo, T.; Kim, D. Excitation Energy Transport Processes of Porphyrin Monomer, Dimer, Cyclic Trimer, and Hexamer Probed by Ultrafast Fluorescence Anisotropy Decay. *Journal of the American Chemical Society* **2003**, *125*, 5849–5860.

(7) Parkinson, P.; Knappke, C. E. I.; Kamonsutthipaijit, N.; Sirithip, K.; Matichak, J. D.; Anderson, H. L.; Herz, L. M. Ultrafast Energy Transfer in Biomimetic Multistrand Nanorings. *Journal of the American Chemical Society* **2014**, *136*, 8217–8220.

(8) Aratani, N.; Osuka, A. Exploration of Giant Functional Porphyrin Arrays. *Bulletin of the Chemical Society of Japan* **2014**, *88*, 1–27, The energy value of the monomer is closest to his plots.

(9) Bressan, G.; Jirasek, M.; Roy, P.; Anderson, H. L.; Meech, S. R.; Heisler, I. A. Population and coherence dynamics in large conjugated porphyrin nanorings. *Chemical Science* **2022**, *13*, 9624–9636.

(10) Yim, D.; Sung, J.; Kim, S.; Oh, J.; Yoon, H.; Sung, Y. M.; Kim, D.; Jang, W.-D. Guest-Induced Modulation of the Energy Transfer Process in Porphyrin-Based Artificial Light Harvesting Dendrimers. *Journal of the American Chemical Society* **2017**, *139*, 993–1002, PMID: 27977172.

(11) Gotfredsen, H.; Deng, J.-R.; Raden, J. M. V.; Righetto, M.; Hergenhahn, J.; Clarke, M.; Bellamy-Carter, A.; Hart, J.; O'Shea, J.; Claridge, T. D. W. et al. Bending a photonic wire into a ring. *Nature Chemistry* **2022**, *14*, 1436–1442.

(12) Patten, P. G. V.; Shreve, A. P.; Lindsey, J. S.; Donohoe, R. J. Energy-Transfer Modeling for the Rational Design of Multiporphyrin Light-Harvesting Arrays. *The Journal of Physical Chemistry B* **1998**, *102*, 4209–4216.

(13) Yang, J.; Yoon, M.-C.; Yoo, H.; Kim, P.; Kim, D. Excitation energy transfer in multiporphyrin arrays with cyclic architectures: towards artificial light-harvesting antenna complexes. *Chemical Society Reviews* **2012**, *41*, 4808–4826.

(14) Herz, L. M.; Silva, C.; Grimsdale, A. C.; Müllen, K.; Phillips, R. T. Time-dependent energy transfer rates in a conjugated polymer guest-host system. *Physical Review B* **2004**, *70*, 165207.

(15) Berberan-Santos, M.; Bodunov, E.; Valeur, B. Mathematical functions for the analysis of luminescence decays with underlying distributions 1. Kohlrausch decay function (stretched exponential). *Chemical Physics* **2005**, *315*, 171–182.

(16) Kundu, S.; Dani, R.; Makri, N. B800-to-B850 relaxation of excitation energy in bacterial light harvesting: All-state, all-mode path integral simulations. *The Journal of Chemical Physics* **2022**, *157*, 015101.

(17) Strümpfer, J.; Schulten, K. Light harvesting complex II B850 excitation dynamics. *The Journal of Chemical Physics* **2009**, *131*, 225101.

(18) Yeh, S.-H.; Zhu, J.; Kais, S. Population and coherence dynamics in light harvesting complex II (LH2). *The Journal of Chemical Physics* **2012**, *137*, 084110.

(19) Runeson, J. E.; Lawrence, J. E.; Mannouch, J. R.; Richardson, J. O. Explaining the Efficiency of Photosynthesis: Quantum Uncertainty or Classical Vibrations? *The Journal of Physical Chemistry Letters* **2022**, *13*, 3392–3399.

(20) Moix, J.; Wu, J.; Huo, P.; Coker, D.; Cao, J. Efficient Energy Transfer in Light-Harvesting Systems, III: The Influence of the Eighth Bacteriochlorophyll on the Dynamics and Efficiency in FMO. *The Journal of Physical Chemistry Letters* **2011**, *2*, 3045–3052.

(21) Wu, J.; Liu, F.; Ma, J.; Silbey, R. J.; Cao, J. Efficient energy transfer in light-harvesting

systems: Quantum-classical comparison, flux network, and robustness analysis. *The Journal of Chemical Physics* **2012**, *137*, 174111.

(22) Kreisbeck, C.; Kramer, T.; Rodriguez, M.; Hein, B. High-Performance Solution of Hierarchical Equations of Motion for Studying Energy Transfer in Light-Harvesting Complexes. *Journal of Chemical Theory and Computation* **2011**, *7*, 2166–2174.

(23) Ishizaki, A.; Fleming, G. R. Theoretical examination of quantum coherence in a photosynthetic system at physiological temperature. *Proceedings of the National Academy of Sciences* **2009**, *106*, 17255–17260.

(24) Gao, J.; Shi, W.-J.; Ye, J.; Wang, X.; Hirao, H.; Zhao, Y. QM/MM Modeling of Environmental Effects on Electronic Transitions of the FMO Complex. *The Journal of Physical Chemistry B* **2013**, *117*, 3488–3495.

(25) Cotton, S. J.; Miller, W. H. The Symmetrical Quasi-Classical Model for Electronically Non-Adiabatic Processes Applied to Energy Transfer Dynamics in Site-Exciton Models of Light-Harvesting Complexes. *Journal of Chemical Theory and Computation* **2016**, *12*, 983–991.

(26) Tanimura, Y. Numerically "exact" approach to open quantum dynamics: The hierarchical equations of motion (HEOM). *The Journal of Chemical Physics* **2020**, *153*, 020901.

(27) Tanimura, Y.; Kubo, R. Two-Time Correlation Functions of a System Coupled to a Heat Bath with a Gaussian-Markoffian Interaction. *Journal of the Physical Society of Japan* **1989**, *58*, 1199–1206.

(28) Yong, C.-K.; Parkinson, P.; Kondratuk, D. V.; Chen, W.-H.; Stannard, A.; Summerfield, A.; Sprafke, J. K.; O'Sullivan, M. C.; Beton, P. H.; Anderson, H. L. et al. Ultrafast delocalization of excitation in synthetic light-harvesting nanorings. *Chemical Science* **2014**, *6*, 181–189.

(29) Yang, J.; Yoon, M.-C.; Yoo, H.; Kim, P.; Kim, D. Excitation energy transfer in multiporphyrin

arrays with cyclic architectures: towards artificial light-harvesting antenna complexes. *Chemical Society Reviews* **2012**, *41*, 4808–4826.

(30) Dreuw, A.; Head-Gordon, M. Single-Reference ab Initio Methods for the Calculation of Excited States of Large Molecules. *Chemical Reviews* **2005**, *105*, 4009–4037.

(31) Lange, A. W.; Herbert, J. M. A smooth, nonsingular, and faithful discretization scheme for polarizable continuum models: The switching/Gaussian approach. *The Journal of Chemical Physics* **2010**, *133*, 244111.

(32) Becke, A. D. Density-functional thermochemistry. III. The role of exact exchange. *The Journal of Chemical Physics* **1993**, *98*, 5648–5652.

(33) Lee, C.; Yang, W.; Parr, R. G. Development of the Colle-Salvetti correlation-energy formula into a functional of the electron density. *Phys. Rev. B* **1988**, *37*, 785–789.

(34) Yanai, T.; Tew, D. P.; Handy, N. C. A new hybrid exchange–correlation functional using the Coulomb-attenuating method (CAM-B3LYP). *Chemical Physics Letters* **2004**, *393*, 51–57.

(35) Grimme, S.; Ehrlich, S.; Goerigk, L. Effect of the damping function in dispersion corrected density functional theory. *Journal of Computational Chemistry* **2011**, *32*, 1456–1465.

(36) He, R.; Li, H.; Shen, W.; Yang, Q.; Li, M. Vibronic fine-structure in the S 0 $\rightarrow$ S 1 absorption spectrum of zinc porphyrin: A Franck–Condon simulation incorporating Herzberg–Teller theory and the Duschinsky effect. *Journal of Molecular Spectroscopy* **2012**, *275*, 61–70.

(37) Sirohiwal, A.; Berraud-Pache, R.; Neese, F.; Izsak, R.; Pantazis, D. A. Accurate Computation of the Absorption Spectrum of Chlorophyll a with Pair Natural Orbital Coupled Cluster Methods. *The Journal of Physical Chemistry B* **2020**, *124*, 8761–8771.

(38) Adamo, C.; Cossi, M.; Barone, V. An accurate density functional method for the study of magnetic properties: the PBE0 model. *Journal of Molecular Structure: THEOCHEM* **1999**, *493*, 145–157.

(39) Shao, Y.; Mei, Y.; Sundholm, D.; Kaila, V. R. I. Benchmarking the Performance of Time-Dependent Density Functional Theory Methods on Biochromophores. *Journal of Chemical Theory and Computation* **2019**, *16*, 587–600.

(40) Weigend, F.; Ahlrichs, R. Balanced basis sets of split valence, triple zeta valence and quadruple zeta valence quality for H to Rn: Design and assessment of accuracy. *Phys. Chem. Chem. Phys.* **2005**, *7*, 3297–3305.

(41) Shao, Y.; Gan, Z.; Epifanovsky, E.; Gilbert, A. T.; Wormit, M.; Kussmann, J.; Lange, A. W.; Behn, A.; Deng, J.; Feng, X. et al. Advances in molecular quantum chemistry contained in the Q-Chem 4 program package. *Molecular Physics* **2015**, *113*, 184–215.

(42) Wohlfarth, C. In *Static Dielectric Constants of Pure Liquids and Binary Liquid Mixtures / Statische Dielektrizitätskonstanten reiner Flüssigkeiten und binärer flüssiger Mischungen*, 1991st ed.; Madelung, O., Ed.; Landolt-Börnstein: Numerical Data and Functional Relationships in Science and Technology - New Series; Springer: Berlin, Germany, 1991.

(43) Adolphs, J.; Renger, T. How Proteins Trigger Excitation Energy Transfer in the FMO Complex of Green Sulfur Bacteria. *Biophysical Journal* **2006**, *91*, 2778–2797.

(44) Ha, J.-H.; Cho, H. S.; Song, J. K.; Kim, D.; Aratani, N.; Osuka, A. Excitonic Coupling Strength and Coherence Length in the Singlet and Triplet Excited States of meso–meso Directly Linked Zn(II)porphyrin Arrays. *ChemPhysChem* **2004**, *5*, 57–67.

(45) Drobizhev, M.; Stepanenko, Y.; Dzenis, Y.; Karotki, A.; Rebane, A.; Taylor, P. N.; Anderson, H. L. Extremely Strong Near-IR Two-Photon Absorption in Conjugated Porphyrin Dimers: Quantitative Description with Three-Essential-States Model. *The Journal of Physical Chemistry B* **2005**, *109*, 7223–7236.

(46) Weiss, U. *Quantum Dissipative Systems*, 4th ed.; World Scientific, 2012; pp 27–28.

(47) Ishizaki, A.; Fleming, G. R. Unified treatment of quantum coherent and incoherent hopping dynamics in electronic energy transfer: Reduced hierarchy equation approach. *The Journal of Chemical Physics* **2009**, *130*, 234111.

(48) Meier, T.; Chernyak, V.; Mukamel, S. Multiple Exciton Coherence Sizes in Photosynthetic Antenna Complexes viewed by PumpProbe Spectroscopy. *The Journal of Physical Chemistry B* **1997**, *101*, 7332–7342.

(49) Roy, P. P.; Kundu, S.; Valdiviezo, J.; Bullard, G.; Fletcher, J. T.; Liu, R.; Yang, S.-J.; Zhang, P.; Beratan, D. N.; Therien, M. J. et al. Synthetic Control of Exciton Dynamics in Bioinspired Cofacial Porphyrin Dimers. *Journal of the American Chemical Society* **2022**, *144*, 6298–6310.

(50) Strumpfer, J.; Schulten, K. Open Quantum Dynamics Calculations with the Hierarchy Equations of Motion on Parallel Computers. *Journal of Chemical Theory and Computation* **2012**, *8*, 2808–2816.

(51) Peeks, M. D.; Neuhaus, P.; Anderson, H. L. Experimental and computational evaluation of the barrier to torsional rotation in a butadiyne-linked porphyrin dimer. *Physical Chemistry Chemical Physics* **2016**, *18*, 5264–5274.

(52) Peter, J. S.; Holzinger, R.; Ostermann, S.; Yelin, S. F. Examining the quantum signatures of optimal excitation energy transfer. *arXiv* **2024**, 2403.00058.

(53) Donehue, J. E.; Varnavski, O. P.; Cemborski, R.; Iyoda, M.; Goodson, T. Probing Coherence in Synthetic Cyclic Light-Harvesting Pigments. *Journal of the American Chemical Society* **2011**, *133*, 4819–4828.

(54) Yang, J.; Yoo, H.; Aratani, N.; Osuka, A.; Kim, D. Determination of the Superradiance Coherence Length of Directly Linked Linear Porphyrin Arrays at the Single-Molecule Level. *Angewandte Chemie* **2009**, *121*, 4387–4391.

(55) Dahlbom, M.; Pullerits, T.; Mukamel, S.; Sundström, V. Exciton Delocalization in the B850 Light-Harvesting Complex: Comparison of Different Measures. *The Journal of Physical Chemistry B* **2001**, *105*, 5515–5524, See the coherence length definition compared to experiments.

(56) Moix, J. M.; Zhao, Y.; Cao, J. Equilibrium-reduced density matrix formulation: Influence of noise, disorder, and temperature on localization in excitonic systems. *Physical Review B* **2012**, *85*, 115412.

(57) Holzinger, R.; Peter, J. S.; Ostermann, S.; Ritsch, H.; Yelin, S. Harnessing quantum emitter rings for efficient energy transport and trapping. *Optica Quantum* **2024**, *2*, 57.

Accepted Manuscript
Version of Record at: https://doi.org/10.1021/acs.jpcc.4c03849

TOC Graphic